


Probing multiferroic order parameters and domain population via nuclear spinsM. Prinz-Zwick ¹, T. Gimpel,¹ K. Geirhos,¹ S. Ghara,¹ C. Steinbrecht,¹ V. Tsurkan,^{1,2} N. Büttgen,¹ and I. Kézsmárki¹¹*Experimental Physics V, Center for Electronic Correlations and Magnetism, University of Augsburg, 86159 Augsburg, Germany*²*Institute of Applied Physics, Chisinau, Republic of Moldova*

(Received 30 July 2021; accepted 13 December 2021; published 6 January 2022)

Quantifying domain population in multiferroics is required to understand domain nucleation/switching processes and achieve on-demand domain control. We report an approach based on nuclear magnetic resonance spectroscopy for the accurate measurement of volume fractions of multiferroic domains in bulk crystals. We demonstrate on a benchmarking system, GaV_4Se_8 , that the electric quadrupole interaction of the ^{71}Ga and the hyperfine field at the ^{51}V nuclei are proper microscopic probes of the ferroelectric polarization and the ferromagnetic moment, respectively. We use the anisotropy of these local quantities to determine the multiferroic domain population, controlled here by both electric and magnetic fields. The sensitivity of this local-probe technique to site symmetries facilitates domain quantification in a wide range of anisotropic magnets, ferroelectrics, and multiferroics.

DOI: [10.1103/PhysRevB.105.014301](https://doi.org/10.1103/PhysRevB.105.014301)**I. INTRODUCTION**

Domains in ferroic materials, that are regions with different orientations of the order parameter, have been found to form versatile architectures with unique functionalities of the domain walls (DWs) separating them [1–10]. Domains emerging in multiferroic materials where magnetic order is accompanied by ferroelectricity or ferroelasticity represent a novel class of domains that is of fundamental interest as cross-coupling phenomena, such as the magnetoelectric effect, can lead to additional functionalities beyond the realm of (mono)ferroic DWs and open up new ways of domain control [11–14].

In type-I multiferroics, where magnetic orders develop within a structurally distorted state, different ferroelectric and/or ferroelastic domain states are also distinguished via their specific microscopic magnetic interactions. Most evidently, the principle axes of magnetic anisotropy, usually linked to the main crystallographic axes, vary between the different structural domain states. This facilitates the control of such domains via magnetic fields [9,10,15] in addition to their more common electric [16] and strain control [17]. Moreover, at atomically sharp structural DWs where the magnetic interactions show a steplike change, new magnetic states can emerge, which are nonexistent in the bulk [9]. In type-II multiferroics where magnetic and ferrodistorive orders emerge hand in hand, the coupling of different degrees of freedom can also lead to complex magnetic states with strong magnetoelectric and/or magnetoelastic effects [13]. This can provide new paths for domain control, such as the interconversion between domains and DWs [18].

Recently, complex domain structures, such as the six-fold vortex domains in ferroelectric hexagonal manganites [19–21] and the magnetic skyrmions in noncentrosymmetric magnets [22–26], have been attracting a great interest

due to their topologically protected structure. In this context, magnetic skyrmions are essentially nanometric cylindrical domains, forming periodic lattices when the DW energy becomes negative due to the Dzyaloshinskii-Moriya interaction [27]. Whether these topologically protected polar or magnetic states can lead to technological breakthroughs in electronics or spintronics depends on our understanding about domain nucleation and stability in such materials. First of all, this requires methods for quantifying domain populations.

Although there have been great advances made in the imaging of structural, ferroelectric, and magnetic domains by techniques that are surface sensitive or limited to small sample thicknesses [28–30], such as scanning probe microscopy methods, second-harmonic generation, high-resolution transmission electron microscopy, magnetic circular dichroism microscopy, methods that are capable of the precise quantification of domain populations in bulk materials are less developed. This is particularly the case for magnetic and multiferroic domains in bulk samples where polarized neutron diffraction is often the only approach to study the domain population [31]. Conventional magnetization and polarization measurements cannot be used to quantify domain populations unless there are only two (\pm) domain states coexisting. This motivates our paper together with former nuclear magnetic resonance (NMR) spectroscopy studies on multiferroics with spiral spin structure [32–35] to demonstrate that multinuclei NMR spectroscopy can probe different order parameter simultaneously and, hence, can provide quantitative information about the volume fractions of different domain states either purely structural or magnetic or both by probing domain-specific microscopic quantities.

In the present paper, we use GaV_4Se_8 as a benchmark system to demonstrate the power of NMR spectroscopy in the quantification of multiferroic domains. This compound belongs to a novel class of multiferroic materials, the lacunar

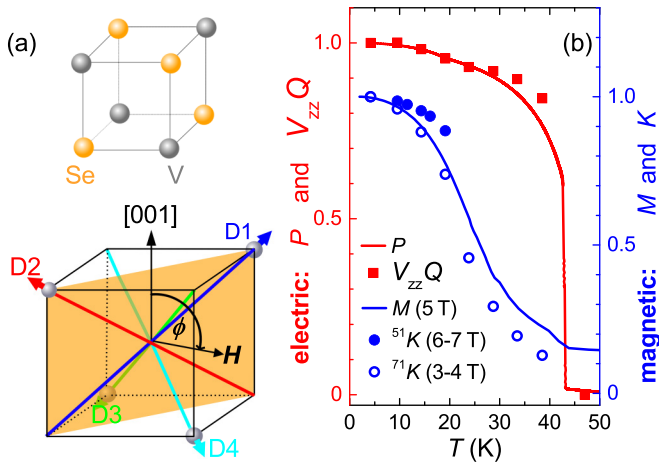


FIG. 1. (a) V_4Se_4 cluster (top) and the four polar/anisotropy axes (bottom) in GaV_4Se_8 . The color code of these axes, $\mathbf{P}_1 = [111]$, $\mathbf{P}_2 = [\bar{1}\bar{1}1]$, $\mathbf{P}_3 = [\bar{1}1\bar{1}]$, and $\mathbf{P}_4 = [1\bar{1}\bar{1}]$, indicates the contributions of the corresponding domain states, D1–D4, in all other figures. \mathbf{H} is rotated within the $(1\bar{1}0)$ plane (orange), where ϕ is the angle between the \mathbf{H} and the $[001]$ axes. (b) Temperature dependence of the quadrupole coupling $eV_{zz}Q/h$ for ^{71}Ga (red symbols), the macroscopic ferroelectric polarization P (red line), the NMR line-shift K for $^{51}V/^{71}Ga$ (full/open blue symbols), and the bulk magnetization M (blue line). (Signal from ^{51}V could be traced only < 20 K due to fast T_2 relaxation). All quantities are normalized by their values at 4 K ($^{51}K = -33.6\%$, $^{71}K = 8.8\%$).

spinel, which have recently attracted attention as the first bulk hosts of Néel-type skyrmions [36–38] that are also dressed with ferroelectric polarization [9,10,39–41].

Lacunar spinels with the chemical formula of AB_4X_8 , crystallize in a cubic structure where two types of clusters AX_4 and B_4X_4 form a NaCl-like lattice. In GaV_4Se_8 , GaV_4Se_8 , and $GaMo_4S_8$, the degeneracy of the B_4X_4 cluster orbitals drives a cooperative Jahn-Teller distortion [40,42–44], which reduces the symmetry from cubic $F\bar{4}3m$ to rhombohedral polar $R3m$.

In GaV_4Se_8 , the polar distortion at $T_{JT} = 42$ K leads to an elongation of the V_4 tetrahedra along one of the four body diagonals of the cubic structure [41]. Due to the lack of inversion symmetry in the parent $F\bar{4}3m$ structure, there are no domains with reversed polarization coexisting ($\pm P$ domains), instead, there are only four domain states with the corresponding polarizations spanning 109° as shown in Fig. 1(a). The polar axis of a given domain is, at the same time, the axis of uniaxial anisotropy [37,45]. Correspondingly, below T_{JT} , there are four domain states each having a distinct magnetic easy axis. Below the magnetic ordering temperature $T_C = 18$ K, GaV_4Se_8 hosts various magnetic phases, including a cycloidal and a Néel-type skyrmion lattice state [37,38,41]. Due to the uniaxial magnetic anisotropy, the magnetic phase diagram depends not only on the magnitude, but also on the orientation of the magnetic field, thus, it is specific to the different domain states [9]. Moreover, due to the axial distortion, the rhombohedral domains can be controlled both via electric and magnetic fields [9,10,15].

Here, we show that in addition to the anisotropic electron spin susceptibility, the rhombohedral distortion in GaV_4Se_8 also leads to an anisotropy of the hyperfine coupling at the

^{51}V nuclei which we exploit to measure the volume fractions of the different rhombohedral polar domains at $T < T_C$ where the compound becomes multiferroic. Moreover, we show that the so-called quadrupole splitting of the ^{71}Ga NMR line as another consequence of the polar distortion offers a complementary path to determine the domain population in GaV_4Se_8 .

II. EXPERIMENTAL TECHNIQUE UTILIZING V_4Se_4 CLUSTER NMR

We recorded field-swept NMR spectra at $\nu = 51$ MHz using a phase-coherent homebuilt spectrometer in a homodyne mode. At first, we investigated an unpoled single crystal of GaV_4Se_8 (with mass 9.22 mg, grown via chemical transport reaction [40], diameter ≈ 1 mm). As demonstrated in Fig. 1(b), NMR studies on ^{51}V (with nuclear spin $I = 7/2$) and ^{71}Ga ($I = 3/2$) provide access to both the electric- and the magnetic-order parameters. The ferroelectric polarization P can be detected via the quadrupole coupling $eV_{zz}Q/h$ that is induced by the interaction of the electric quadrupole moment Q of the ^{71}Ga nucleus with the local electric-field gradient V_{zz} [46], emerging below T_{JT} . The magnetization and its orientation can be probed locally via the line-shift K of ^{51}V and ^{71}Ga nuclei, originating from the internal magnetic field of the unpaired d electron at the V_4 cluster, shown in Fig. 1(a). Figures S1 and S2 in the Supplemental Material [47] display the spectra from which these parameters were extracted.

In all experiments, the applied magnetic-field \mathbf{H} , irrespective of its orientation, was strong enough to set the material to the field-polarized ferromagnetic state with the electron magnetization being parallel to the field [37,41]. Thus, the dependence of the NMR spectra on the orientation of \mathbf{H} , that was rotated within the $(1\bar{1}0)$ crystallographic plane [see Fig. 1(a)], fully originates from the anisotropy of the hyperfine coupling, induced by the polar rhombohedral distortion. The population of the multiferroic domains was controlled by poling the crystals through T_{JT} using static electric or magnetic fields. Due to fast T_2 relaxation of the ^{51}V nuclei, a rather short pulse sequence was chosen, using 4- μs solid-echo pulses separated by a 25- μs pulse separation time.

The rhombohedral transition is expected to split the ^{51}V line into four peaks for arbitrary directions of \mathbf{H} , where each peak is associated with one type of domain. In fact, Figs. 2(a) and 2(b) reveal an unusually strong anisotropy of the hyperfine field at 4.2 K. Four ^{51}V lines, one for each domain state, are resolved and the resonance fields vary within $4.6 < \mu_0 H_{Res} < 7.3$ T.

Upon the rotation of \mathbf{H} within the $(1\bar{1}0)$ plane as sketched in Fig. 1(a), the field passes through the anisotropy (polar) axes of the D1 and D2 domains. For these two domains, the resonance field curve in Fig. 2(a) passes through a minimum/maximum when \mathbf{H} is parallel/perpendicular to the anisotropy axis. For the other two domain states, the angle spanned by \mathbf{H} and their anisotropy axes varies between 54° and 90° upon the rotation of \mathbf{H} , thus, only the maximum of H_{Res} is observed. Ideally, the resonance-field curves of these D3 and D4 domains should fully overlap, and all four curves should cross each other when \mathbf{H} points along the $[001]$ axis. Deviations from this behavior are caused by a small misalignment of $\sim 4^\circ$, which allows us to resolve four distinct lines at

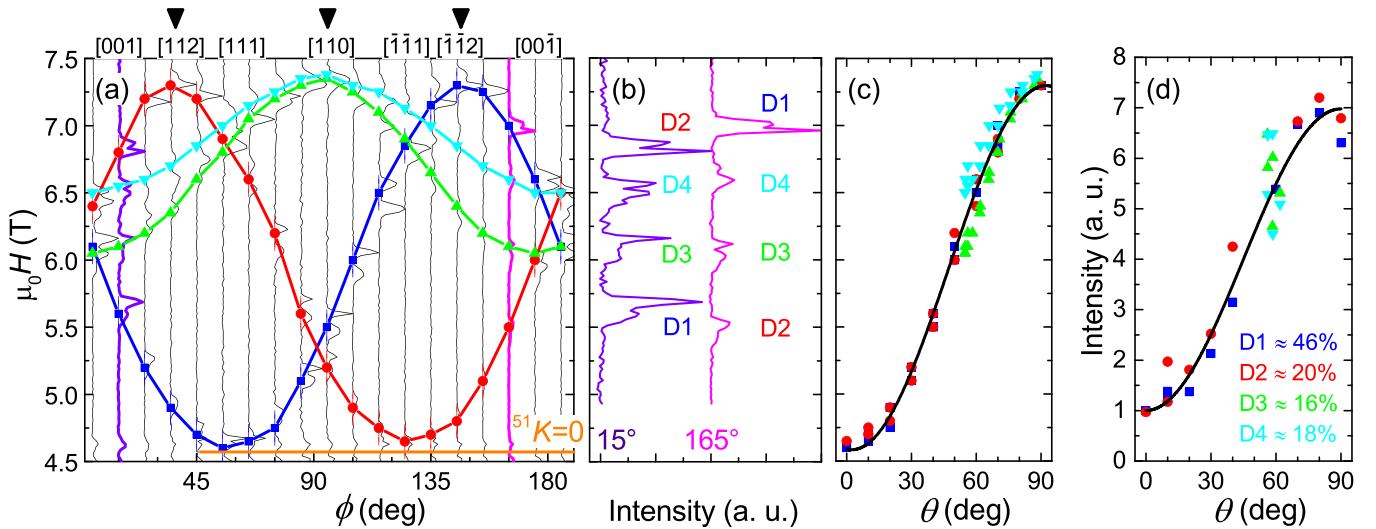


FIG. 2. (a) Dependence of the ^{51}V NMR spectra on the orientation of \mathbf{H} , at 51 MHz at 4.2 K. Individual field-swept spectra (gray lines) are displayed at the respective angles. Spectra at $\phi = 15^\circ$ and 165° , respectively, highlighted by purple and pink colors, are enlarged in panel (b). The angular dependence of the ^{51}V resonance fields corresponding to domains D–D4, are traced by lines with colors chosen according to Fig. 1(a). The diamagnetic reference field $^{51}\text{K} = 0$ of the ^{51}V nuclei is shown by the horizontal orange line. (c)/(d) Resonance field H_{res} /intensity I versus θ , the angle spanned by \mathbf{H} and the polar axes of the respective domains. In panel (d), the intensity values for the different domains are scaled according to the percentages indicated in the figure, which correspond to the volume fraction of the domains. Solid black lines indicate the $\sin^2 \theta$ dependence of H_{res} . Panels (a)–(c) share a common vertical scale. All data were collected on an unpoled crystal.

arbitrary orientations of \mathbf{H} as exemplified by two spectra in Fig. 2(b).

Intensities of the four lines contain information about the volume fractions of the four domains. However, the volume fraction is not the only factor determining the relative intensities since they also vary with the orientation of \mathbf{H} as obvious from Fig. 2(b), which can also be followed in Fig. 2(d). To reveal the angular dependence of the line intensities, in Figs. 2(c) and 2(d), we plot the fields H_{res} and the intensities of the four lines versus the angle θ , spanned by \mathbf{H} with the anisotropy axes of the corresponding domains. The resonance field follows an angular dependence common for all domains, according to $H_{\text{res}}(\theta) = H_0 + A \sin^2 \theta$, where $\mu_0 H_0 = 4.55$ T is the resonance field of the diamagnetic ^{51}V nucleus at 51 MHz and A is the anisotropy of the hyperfine field. Since H_{res} is always higher than or equal to H_0 , the local internal field at the ^{51}V nuclei points opposite to the applied field. The internal field at the ^{51}V nuclei likely originates from the magnetic moment of the unpaired electron on the same V_4 cluster via contact and dipolar terms, whereas intercluster hyperfine interactions likely give a minor contribution, similar to GaV_4S_8 [48,49].

The intensities of all domains follow the same angular dependence of H_{res} , i.e., they also exhibit a simple $\propto \sin^2 \theta$ dependence as demonstrated in Fig. 2(d). Therefore, the intensity curves all collapse on each other after normalization. Importantly, the angular-independent normalization factors lead to the volume fractions, listed as a legend in Fig. 2(d).

As additionally seen in Fig. 2(b), all four ^{51}V lines exhibit weak splittings due to quadrupolar interactions and the inequivalence of vanadium sites within the distorted V_4 clusters. Since these splittings, partly resolved in the field-swept spectra, are not relevant in the process of domain quantifica-

tion, the overall intensities of the four lines were obtained by integration over these fine structures.

III. DOMAIN QUANTIFICATION UNDER ELECTRIC AND MAGNETIC DOMAIN CONTROLS

Next, we describe a more precise approach for domain quantification where the angular dependence of the intensity does not play a role and the line intensities directly measure the volume fractions of the corresponding domain states, reducing possible errors caused by misalignments or low signal/noise ratios for small polar angles in the previous semi-quantitative approach. In the second scheme, the NMR spectra are measured in such configurations that the same orientation of \mathbf{H} with respect to the anisotropy axis is realized for each domain state in one of the configurations. As seen in Fig. 2(a) when the field is rotated within the $(1\bar{1}0)$ plane, there are three configurations where \mathbf{H} is perpendicular to some of the four anisotropy axes, thus, the resonance fields of the corresponding domains are the same. This holds for the D2 and the D1 domains at $\phi = 35^\circ$ and 145° , respectively, and for both the D3 and the D4 domains at 90° . Under this condition, the relative intensities depend solely on the domain population, whereas angular-dependent effects, coming, e.g., from T_2 relaxation, cancel out. Hence, by comparing the intensities of the lines at these three angles, where they are located at the maximum $\mu_0 H_{\text{res}} \approx 7.3$ T, one can uniquely determine the volume fractions of the D1 and the D2 domains and the sum of the D3 and the D4 domains as presented in the middle column of Fig. 3(a). Note that the percentages roughly agree with those given in Fig. 2(d), whereas the previous approach has larger uncertainties. Next, this method is used to trace changes in domain population upon electric or magnetic control.

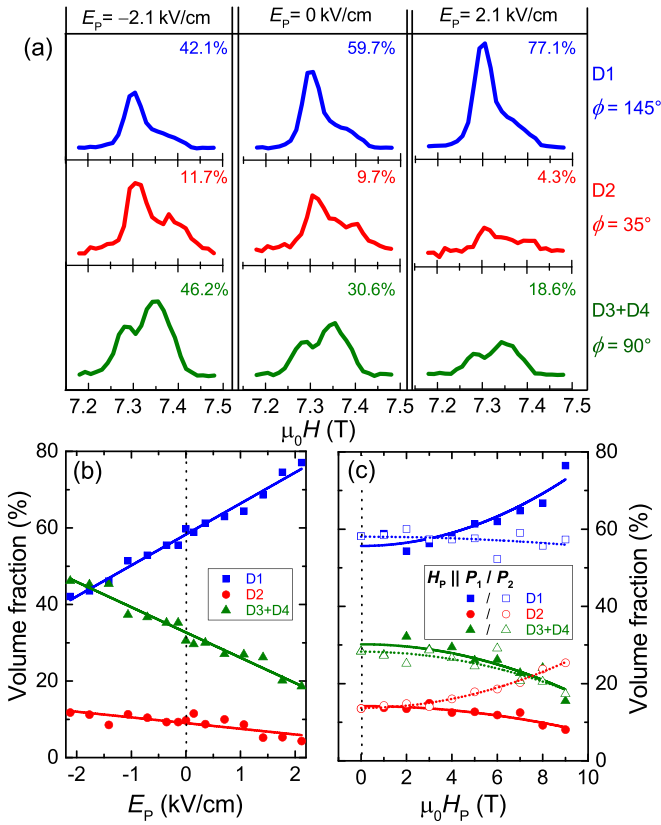


FIG. 3. (a) ^{51}V spectra of different domains measured after electric poling with three different strengths of $\mathbf{E}_p \parallel \mathbf{P}_1$. Data for each poling are in separate columns. The spectra of different domains, in separate rows, were measured at such orientations of \mathbf{H} where the resonance field is the maximal $H_{\text{res}} = 7.3$ T for the corresponding domain [D1: $\phi = 145^\circ$, D2: $\phi = 35^\circ$, D3 + D4: $\phi = 90^\circ$, see black top arrows in Fig. 2(a)]. Although spectra in each row are plotted on a common intensity scale to track poling induced changes in the population of the corresponding domains, the intensity scales of the different rows are chosen arbitrarily to optimize visibility. The relative intensities of all lines, i.e., the volume fractions of the respective domains, are given in percentages. (b) and (c) Volume fractions of the different domain states as a function of the poling electric/magnetic-field E_p/H_p . In the latter, results of poling with both $\mathbf{H}_p \parallel \mathbf{P}_1$ and $\mathbf{H}_p \parallel \mathbf{P}_2$ are shown. The linear/quadratic fits correspond to the linear/quadratic E/H dependence of the free energy, which is reflected in the poling efficiency [15].

The domain population was controlled by cooling the sample through T_{JT} , whereas applying poling electric or magnetic fields along the [111] axis, the anisotropy/polar axes of the D1 domain. Correspondingly, one expects the promotion and the suppression of this domain state by positive and negative electric fields, respectively [15]. Figure 3(a) shows that the D1 domain is naturally favored, i.e., it has the largest population even without electric poling, and its population follows the tendency expected for positive and negative poling electric fields. The effect of electric poling on all domain states can be observed in more details in Fig. 3(b). In contrast, the effect of magnetic poling should not depend on the sign of the poling field as the magnetic anisotropy energy is an even function of \mathbf{H} [15]. Indeed, we observe in Fig. 3(c) that the populations of

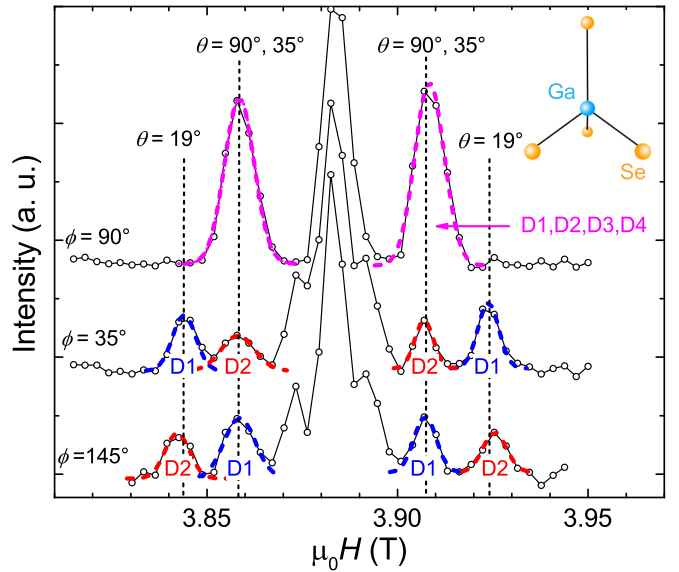


FIG. 4. ^{71}Ga spectra at 38.5 K and 51 MHz for three orientations of the magnetic-field $\phi = 35^\circ$, 90° and 145° . In addition to the central line at ~ 3.88 T, quadrupolar satellites are resolved. Values of θ , i.e., the angle between \mathbf{H} and the polar axes of the domains, are indicated for each satellite pair together with the domains contributing to the satellites.

the different domains change quadratically with the magnetic field.

Our microscopic domain quantification method was validated via the simultaneous investigation of the domain population using macroscopic pyroelectric current measurement (for more details, see Fig. S3 of the supplemental Material [47]). However, this macroscopic control method has strong limitations as it cannot quantify the fraction of the different domain states (D1 \dots D4) separately. Instead, it measures the overall polarization P , that is related to the individual volume fractions V according to $P = P_0[V_{\text{D1}} - (V_{\text{D2}} + V_{\text{D3}} + V_{\text{D4}}) \cos 71^\circ]$, where P_0 is the magnitude of the saturation polarization.

We carried out another independent validation of the domain quantification technique using the other nuclear probe, namely, the quadrupole splitting of ^{71}Ga . In the finite magnetic field, the ^{71}Ga line splits into three lines: A central line and two symmetric satellites. In the field-swept spectrum, the distance between the two satellite lines is given by [46]

$$\Delta H = \frac{3\pi eV_{zz}Q}{\gamma h I(2I - 1)}(3 \cos^2 \theta - 1). \quad (1)$$

Note that ΔH carries domain-specific information as an arbitrarily orientated field spans different angles with the polar axes of the domains. In strong contrast to the low-temperature behavior of the ^{51}V spectrum, the ^{71}Ga spectrum at temperatures $T_C < T < T_{\text{JT}}$ is governed by the quadrupole splitting as the anisotropy of the hyperfine coupling is negligible, thus, the angular dependence of the spectra are well described by Eq. (1).

The domain quantification is demonstrated in Fig. 4, where three ^{71}Ga spectra of an unpoled crystal are shown for $\phi = 90^\circ$, 35° , and 145° , the angles highlighted by black arrows

in Fig. 2(a). For the first angle, we only expect and observe two satellites since ΔH has the same value for all four domains. In the $\phi = 35^\circ$ and 145° spectra, the satellites of the D1 and D2 domains can be resolved separately, whereas the satellites of D3 and D4 domains strongly overlap with the central peak. From these three spectra the volume fractions of the domains can be determined, $D1 \approx 28\%$, $D2 \approx 20\%$, and $D3 + D4 \approx 52\%$. These values closely reproduce those obtained within the same cooling run using the former procedure based on the anisotropic hyperfine coupling of ^{51}V , namely, $D1 \approx 27\%$, $D2 \approx 21\%$, and $D3 + D4 \approx 52\%$.

IV. CONCLUSION

In conclusion, we developed a method for the quantification of domain populations in bulk magnetic, ferroelectric, and/or ferroelastic as well as multiferroic crystals. Domains are selectively probed via the distinct response of the nuclear spins in the different domains. In externally applied magnetic fields, the NMR spectrum becomes domain specific since it depends on the relative orientation of the order parameters and the external field, which has been exploited to determine

the fraction of spin spirals with different ordering vectors [32–35]. In GaV_4Se_8 , we demonstrate that magnetic domains are easily distinguishable via the anisotropy of the hyperfine coupling since the orientation of the anisotropy axes are dictated by domain-specific lattice distortions. Similarly, domains are also efficiently distinguished by the orientation of the local electric-field gradient at polar sites, probed via nuclear quadrupole interaction. The former approach is applicable to any nucleus, whereas the second one requires nuclei with finite quadrupole moments. The possibility to probe the magnetic and electric order parameters simultaneously can give a microscopic insight into the origin of multiferroicity in new systems. Concerning symmetry requirements, these methods can work whenever the crystal symmetry is lower than cubic, which is the case for ferroic domains, in general. Thus, our method is applicable for a wide range of materials.

ACKNOWLEDGMENTS

This work was supported by the German Research Foundation (DFG) via Projects No. 107745057 (TRR80) and No. KE 2370/3-1.

-
- [1] A. K. Tagantsev, L. E. Cross, and J. Fousek, *Domains in Ferroic Crystals and Thin Films* (Springer, New York, 2010), Vol. 13.
- [2] A. Aird and E. K. Salje, Sheet superconductivity in twin walls: Experimental evidence of WO_{3-x} , *J. Phys.: Condens. Matter* **10**, L377 (1998).
- [3] P. Zubko, G. Catalan, P. R. L. Welche, A. Buckley, and J. F. Scott, Strain-Gradient-Induced Polarization in SrTiO_3 Single Crystals, *Phys. Rev. Lett.* **99**, 167601 (2007).
- [4] J. Seidel, L. W. Martin, Q. He, Q. Zhan, Y.-H. Chu, A. Rother, M. Hawkrige, P. Maksymovych, P. Yu, M. Gajek *et al.*, Conduction at domain walls in oxide multiferroics, *Nat. Mater.* **8**, 229 (2009).
- [5] S. Van Aert, S. Turner, R. Delville, D. Schryvers, G. Van Tendeloo, and E. K. Salje, Direct observation of ferroelectricity at ferroelastic domain boundaries in CaTiO_3 by electron microscopy, *Adv. Mater.* **24**, 523 (2012).
- [6] E. Y. Ma, Y.-T. Cui, K. Ueda, S. Tang, K. Chen, N. Tamura, P. M. Wu, J. Fujioka, Y. Tokura, and Z.-X. Shen, Mobile metallic domain walls in an all-in-all-out magnetic insulator, *Science* **350**, 538 (2015).
- [7] S. Yun, K. Song, K. Chu, S.-Y. Hwang, G.-Y. Kim, J. Seo, C.-S. Woo, S.-Y. Choi, and C.-H. Yang, Flexopiezoelectricity at ferroelastic domain walls in WO_3 films, *Nat. Commun.* **11**, 4898 (2020).
- [8] S. Farokhipoor, C. Magén, S. Venkatesan, J. Íñiguez, C. J. Daumont, D. Rubi, E. Snoeck, M. Mostovoy, C. De Graaf, A. Müller *et al.*, Artificial chemical and magnetic structure at the domain walls of an epitaxial oxide, *Nature (London)* **515**, 379 (2014).
- [9] K. Geirhos, B. Gross, B. G. Szigeti, A. Mehlin, S. Philipp, J. S. White, R. Cubitt, S. Widmann, S. Ghara, P. Lunkenheimer, V. Tsurkan, E. Neuber, D. Ivaneyko, P. Milde, L. M. Eng, A. O. Leonov, S. Bordacs, M. Poggio, and I. Kezsmarki, Macroscopic manifestation of domain-wall magnetism and magnetoelectric effect in a neel-type skyrmion host, *npj Quantum Mater.* **5**, 44 (2020).
- [10] S. Ghara, K. Geirhos, L. Kuerten, P. Lunkenheimer, V. Tsurkan, M. Fiebig, and I. Kézsmárki, Giant conductivity of mobile non-oxide domain walls, *Nat. Commun.* **12**, 3975 (2021).
- [11] S. Lee, W. Ratcliff, S.-W. Cheong, and V. Kiryukhin, Electric field control of the magnetic state in BiFeO_3 single crystals, *Appl. Phys. Lett.* **92**, 192906 (2008).
- [12] J. T. Heron, M. Trassin, K. Ashraf, M. Gajek, Q. He, S. Y. Yang, D. E. Nikonov, Y. H. Chu, S. Salahuddin, and R. Ramesh, Electric-Field-Induced Magnetization Reversal in a Ferromagnet-Multiferroic Heterostructure, *Phys. Rev. Lett.* **107**, 217202 (2011).
- [13] Y. Tokunaga, N. Furukawa, H. Sakai, Y. Taguchi, T.-h. Arima, and Y. Tokura, Composite domain walls in a multiferroic perovskite ferrite, *Nature Mater.* **8**, 558 (2009).
- [14] N. Leo, A. Bergman, A. Cano, N. Poudel, B. Lorenz, M. Fiebig, and D. Meier, Polarization control at spin-driven ferroelectric domain walls, *Nat. Commun.* **6**, 6661 (2015).
- [15] K. Geirhos, S. Reschke, S. Ghara, S. Krohns, P. Lunkenheimer, and I. Kézsmárki, Optical, dielectric, and magnetoelectric properties of ferroelectric and antiferroelectric lacunar spinels, *Phys. Status Solidi B*, 2100160 (2021).
- [16] D. Meier, Functional domain walls in multiferroics, *J. Phys.: Condens. Matter* **27**, 463003 (2015).
- [17] A. Alsubaie, P. Sharma, J. H. Lee, J. Y. Kim, C.-H. Yang, and J. Seidel, Uniaxial strain-controlled ferroelastic domain evolution in BiFeO_3 , *ACS Appl. Mater. Interfaces* **10**, 11768 (2018).
- [18] E. Hassanpour, M. C. Weber, Y. Zemp, L. Kuerten, A. Bortis, Y. Tokunaga, Y. Taguchi, Y. Tokura, A. Cano, T. Lottermoser, and M. Fiebig, Interconversion of multiferroic domains and domain walls, *Nat. Commun.* **12**, 2755 (2021).

- [19] T. Choi, Y. Horibe, H. Yi, Y. J. Choi, W. Wu, and S.-W. Cheong, Insulating interlocked ferroelectric and structural antiphase domain walls in multiferroic YMnO₃, *Nature Mater.* **9**, 253 (2010).
- [20] D. Meier, J. Seidel, A. Cano, K. Delaney, Y. Kumagai, M. Mostovoy, N. A. Spaldin, R. Ramesh, and M. Fiebig, Anisotropic conductance at improper ferroelectric domain walls, *Nature Mater.* **11**, 284 (2012).
- [21] W. Wu, Y. Horibe, N. Lee, S.-W. Cheong, and J. R. Guest, Conduction of Topologically Protected Charged Ferroelectric Domain Walls, *Phys. Rev. Lett.* **108**, 077203 (2012).
- [22] S. Mühlbauer, B. Binz, F. Jonietz, C. Pfleiderer, A. Rosch, A. Neubauer, R. Georgii, and P. Böni, Skyrmion lattice in a chiral magnet, *Science* **323**, 915 (2009).
- [23] S. Seki, X. Yu, S. Ishiwata, and Y. Tokura, Observation of skyrmions in a multiferroic material, *Science* **336**, 198 (2012).
- [24] N. Nagaosa and Y. Tokura, Topological properties and dynamics of magnetic skyrmions, *Nat. Nanotechnol.* **8**, 899 (2013).
- [25] M. Garst, J. Waizner, and D. Grundler, Collective spin excitations of helices and magnetic skyrmions: Review and perspectives of magnonics in non-centrosymmetric magnets, *J. Phys. D: Appl. Phys.* **50**, 293002 (2017).
- [26] N. Kanazawa, S. Seki, and Y. Tokura, Noncentrosymmetric magnets hosting magnetic skyrmions, *Adv. Mater.* **29**, 1603227 (2017).
- [27] A. Bogdanov and A. Hubert, Thermodynamically stable magnetic vortex states in magnetic crystals, *J. Magn. Magn. Mater.* **138**, 255 (1994).
- [28] E. Neuber, P. Milde, A. Butykai, S. Bordacs, H. Nakamura, T. Waki, Y. Tabata, K. Geirhos, P. Lunkenheimer, I. Kézsmárki, P. Ondrejko, J. Hlinka, and L. M. Eng, Architecture of nanoscale ferroelectric domains in GaMo₄S₈, *J. Phys.: Condens. Matter* **30**, 445402 (2018).
- [29] C. J. Roh, S. Y. Hamh, C. S. Woo, K. E. Kim, C. H. Yang, and J. S. Lee, Ferroelectric domain states of a tetragonal BiFeO₃ thin film investigated by second harmonic generation microscopy, *Nanoscale Res. Lett.* **12**, 353 (2017).
- [30] P. Fischer, T. Eimüller, R. Kalchgruber, G. Schütz, G. Schmahl, P. Guttmann, and G. Bayreuther, X-ray magnetic circular dichroism used to image magnetic domains, *J. Synchrotron Radiat.* **6**, 688 (1999).
- [31] V. Hutanu, A. P. Sazonov, M. Meven, G. Roth, A. Gukasov, H. Murakawa, Y. Tokura, D. Szaller, S. Bordács, I. Kézsmárki, V. K. Guduru, L. C. J. M. Peters, U. Zeitler, J. Romhányi, and B. Nafradi, Evolution of two-dimensional antiferromagnetism with temperature and magnetic field in multiferroic Ba₂CoGe₂O₇, *Phys. Rev. B* **89**, 064403 (2014).
- [32] A. V. Zalesskii, A. K. Zvezdin, I. S. Zheludev, A. M. Savvinov, and A. F. Lebedev, A new type of domain wall NMR spectrum in canted antiferromagnets: YFeO₃ and LuFeO₃ crystals, *Phys. Status Solidi B* **73**, 317 (1976).
- [33] A. V. Zalessky, A. A. Frolov, T. A. Khimich, A. A. Bush, V. S. Pokatilov, and A. K. Zvezdin, ⁵⁷Fe NMR study of spin-modulated magnetic structure in BiFeO₃, *Europhys. Lett.* **50**, 547 (2000).
- [34] D. F. Khozeev, A. V. Zalessky, A. A. Gippius, E. N. Morozova, and A. A. Bush, Spin modulation of ⁵⁷Fe NMR frequency and relaxation in BiFeO₃, *Physica B* **329-333**, 848 (2003).
- [35] Y. A. Sakhratov, L. E. Svistov, P. L. Kuhns, H. D. Zhou, and A. P. Reyes, Magnetic structure and domain conversion of the quasi-2D frustrated antiferromagnet CuCrO₂ probed by NMR, *J. Exp. Theor. Phys.* **119**, 880 (2014).
- [36] I. Kezsmarki, S. Bordacs, P. Milde, E. Neuber, L. M. Eng, J. S. White, H. M. Ronnow, C. D. Dewhurst, M. Mochizuki, K. Yanai, H. Nakamura, D. Ehlers, V. Tsurkan, and A. Loidl, Neel-type skyrmion lattice with confined orientation in the polar magnetic semiconductor GaV₄S₈, *Nature Mater.* **14**, 1116 (2015).
- [37] S. Bordacs, A. Butykai, B. G. Szigeti, J. S. White, R. Cubitt, A. O. Leonov, S. Widmann, D. Ehlers, H. A. K. von Nidda, V. Tsurkan, A. Loidl, and I. Kezsmarki, Equilibrium skyrmion lattice ground state in a polar easy-plane magnet, *Sci. Rep.* **7**, 7584 (2017).
- [38] B. Gross, S. Philipp, K. Geirhos, A. Mehlin, S. Bordacs, V. Tsurkan, A. Leonov, I. Kezsmarki, and M. Poggio, Stability of Neel-type skyrmion lattice against oblique magnetic fields in GaV₄S₈ and GaV₄Se₈, *Phys. Rev. B* **102**, 104407 (2020).
- [39] E. Ruff, S. Widmann, P. Lunkenheimer, V. Tsurkan, S. Bordács, I. Kézsmárki, and A. Loidl, Multiferroicity and skyrmions carrying electric polarization in GaV₄S₈, *Sci. Adv.* **1**, e1500916 (2015).
- [40] E. Ruff, A. Butykai, K. Geirhos, S. Widmann, V. Tsurkan, E. Stefanet, I. Kezsmarki, A. Loidl, and P. Lunkenheimer, Polar and magnetic order in GaV₄Se₈, *Phys. Rev. B* **96**, 165119 (2017).
- [41] Y. Fujima, N. Abe, Y. Tokunaga, and T. Arima, Thermodynamically stable skyrmion lattice at low temperatures in a bulk crystal of lacunar spinel GaV₄Se₈, *Phys. Rev. B* **95**, 180410(R) (2017).
- [42] R. Pocha, D. Johrendt, and R. Pottgen, Electronic and structural instabilities in GaV₄S₈ and GaMo₄S₈, *Chem. Mater.* **12**, 2882 (2000).
- [43] R. Pocha, D. Johrendt, B. F. Ni, and M. M. Abd-Elmeguid, Crystal structures, electronic properties, and pressure-induced superconductivity of the tetrahedral cluster compounds GaNb₄S₈, GaNb₄Se₈, and GaTa₄Se₈, *J. Am. Chem. Soc.* **127**, 8732 (2005).
- [44] A. Butykai, S. Bordacs, I. Kezsmarki, V. Tsurkan, A. Loidl, J. Doring, E. Neuber, P. Milde, S. C. Kehr, and L. M. Eng, Characteristics of ferroelectric-ferroelastic domains in Neel-type skyrmion host GaV₄S₈, *Sci. Rep.* **7**, 44663 (2017).
- [45] D. Ehlers, I. Stasinopoulos, I. Kézsmárki, T. Fehér, V. Tsurkan, H.-A. K. von Nidda, D. Grundler, and A. Loidl, Exchange anisotropy in the skyrmion host GaV₄S₈, *J. Phys.: Condens. Matter* **29**, 065803 (2016).
- [46] C. P. Slichter, *Principles of Magnetic Resonance* (Springer-Verlag, New York/Heidelberg/Berlin, 1978).
- [47] See Supplemental Material at <http://link.aps.org/supplemental/10.1103/PhysRevB.105.014301> for figures containing the temperature dependence of the ⁷¹Ga and ⁵¹V spectra, the comparison between NMR and polarization data and a picture of the investigated single crystal.
- [48] H. Nakamura, H. Chudo, M. Shiga, and T. Kohara, Split and compensated hyperfine fields in magnetic metal clusters, *Hyperfine Interact.* **159**, 71 (2004).
- [49] H. Nakamura, H. Chudo, and M. Shiga, Structural transition of the tetrahedral metal cluster: nuclear magnetic resonance study of GaV₄S₈, *J. Phys. Condens. Matter* **17**, 6015 (2005).